EPJ Web of Conferences **71**, 00022 (2014)
DOI: 10.1051/epjconf/20147100022

Forward Physics at CMS

Grzegorz Brona[1,a] for CMS Collaboration.

[1] *Warsaw University, Faculty of Physics, Hoza 69, Warsaw, Poland*

Abstract. An overview of the forward physics programme at CMS is given. It covers measurements of the central exclusive production, diffractive dissociation, forward energy flow and forward jets.

1 Introduction

Compact Muon Solenoid (CMS) is one of the two large, multi-purpose experiments at the Large Hadron Collider (LHC) at CERN. With a close cooperation with TOTEM experiment, located at the same interaction point, almost 100% coverage in pseudorapirities for charged and neutral particles is assured.

The central part of CMS, which spans to $|\eta| < 3$, is optimized for processes with large polar angles and high values of p_T. It consists of a tracker, hadronic and electromagnetic calorimeters and muon chambers. In the region $|\eta| < 1.74$, the Hadronic Calorimeter (HCAL) cells have widths of 0.087 in η and 0.087 rad in ϕ. In the (η, ϕ) plane, and for $|\eta| < 1.48$, the HCAL cells map on to 5×5 ECAL crystals arrays to form calorimeter towers. At larger values of $|\eta|$, the size of the towers increases and the matching ECAL arrays contain fewer crystals. ECAL and HCAL extend to $|\eta| < 3.0$. In the forward region CMS is complemented by several subdetectors. The two Hadronic Forward (HF) calorimeters cover the region of $3.0 < |\eta| < 5.2$. They consist of iron absorbers and embedded radiation hard quartz fibres, which provide a fast collection of Cerenkov light. Half of the fibres run over the full depth of the absorber, while the other half start at a depth of 22 cm from the front of the detector. This structure makes it possible to distinguish showers generated by electrons and photons, from those generated by hadrons. The tower segmentation of the HF calorimeters in η and ϕ is 0.175×0.175 except for $|\eta|$ above 4.7 where the segmentation is 0.175×0.135. The CMS CASTOR calorimeter is located 14 meters from the interaction point only at one side of the detector and covers range of $-5.2 > \eta > -6.6$. It is a sampling calorimeter with tungsten absorber plates and fused silica plates as an active medium. It is composed of two parts - an electromagnetic one, 22 radiation length deep, and a hadronic one. The total depth is 10.3 interaction lengths. CASTOR is segmented only in ϕ. The CMS Zero Degree Calorimeters (ZDC) are installed at the end of straight beam line section, 140 meters from the interaction point, at both sides of the detector. They are able to detect neutrals, and cover $|\eta| > 8.1$. The $6 < |\eta| < 8$ region is covered by Forward Shower Counters (FSC), which role is to detect an activity at large rapidities and selects events with diffractive gaps at one or two sides of the interaction point.

[a] e-mail: gbrona@fuw.edu.pl

With such a large acceptance CMS is a perfect tool to study a wide range of proton-proton interactions phenomena. The forward physics programme at the CMS, is focused at physics that can be reached with detectors located at $|\eta| > 3.0$. It covers such aspects as central exclusive production (forward detectors used as a veto), double and single diffractive dissociation (forward detectors used to select events with rapidity gap), multiparton interactions and forward jets production.

2 Central exclusive production (CEP)

The CEP is a process of the type: $pp \to p + X + p$ with X being a well defined system e.g. di-lepton or di-jet. The "+" sign denotes the absence of additional activity between the outgoing protons and X. The final state consists of the scattered protons, that survive the interaction intact, and of the system X or its decay products. In the CEP three distinct processes may be involved, namely photon-photon, photon-pomeron and pomeron-pomeron interactions. The system X is reconstructed in the central CMS barrel, while forward detectors are used to veto non-exclusive events.

The CEP of di-photons provides information on several ingredients needed for the exclusive Higgs search, that is on the unintegrated gluon distribution $g(x1, x2)$, the Sudakhov form factor (i.e. the probability of no gluon radiation) and on the rapidity gap survival probability S^2 (i.e. the probability of no other parton-parton interactions). The measured cross section for exclusive di-photons will give an estimation what CEP H cross section to expect. When the exclusive H is found, the ratio $H/(gg)$ (corrected for kinematic dependencies) will determine the ggH coupling in a unique way. In the analysis of 2010 7 TeV data [1] the following requirements were applied: two γ within $|\eta| < 2.5$ and $E_T > 5.5$ GeV, no additional activity within $|\eta| < 5.2$ acceptance. No CEP di-photon candidates defined with those requirements were found. In Fig. 1 the 95% CL limit on the $pp \to p + \gamma\gamma + p$ production cross section is presented and compared with ExHuMe model at LO and NLO.

Exclusive di-lepton production ($\gamma\gamma \to l^+l^-$) is a nearly pure QED process Therefore its cross section is precisely known. Its measurement at the LHC is an independent cross check of the the absolute luminosity calibration. Two exclusive di-lepton analyses were performed on 2010 low pile-up data, production of ee [1] and $\mu\mu$ [2]. For ee channel both leptons were required to have $E_T > 5.5$ GeV and contained within $|\eta| < 2.1$, while for $\mu\mu$ channel $p_T > 4$ GeV, $|\eta| < 2.5$ and $m(\mu\mu) > 11.5$ GeV selection criteria were applied. For ee analysis 17 candidates were found with the Standard Model predictions of $16.3 \pm 1.3(\text{signal}) + 0.85 \pm 0.28(\text{background})$ events. For $\mu\mu$ the production cross section was calculated: $\sigma(pp \to p + \mu\mu + p) = 3.38^{+0.58}_{-0.55}(\text{stat.}) \pm 0.16(\text{syst.}) \pm 0.14(\text{lumi.})$ pb. The data to theory ratio is $0.83^{+0.14}_{-0.13}(\text{stat.}) \pm 0.04(\text{syst.}) \pm 0.03(\text{lumi.})$.

3 Soft diffraction

Inclusive diffractive interactions cannot be calculated within perturbative quantum chromodynamics, and traditionally have been described by models based on Regge theory. The predictions of these models generally differ when extrapolated from pre-LHC center-of-mass energies to 7 TeV at LHC. Therefore, measurements of diffractive cross sections at the LHC provide a valuable input for understanding diffraction and improve its modeling in current event generations. They are also crucial for the proper modeling of the final state of minimum-bias (MB) events, and can help improve the simulation of, e.g., the underlying event, pileup events, and the measurement of the machine luminosity at the LHC.

With 2010 7 TeV low pile-up data CMS performed an analysis of inclusive diffractive cross section, based on the presence of a Large Rapidity Gap (LRG) in pseudorapidity space [3]. The Single Diffractive Dissotiation (SD) and Double Diffractive Dissotiation (DD) events are separated using the

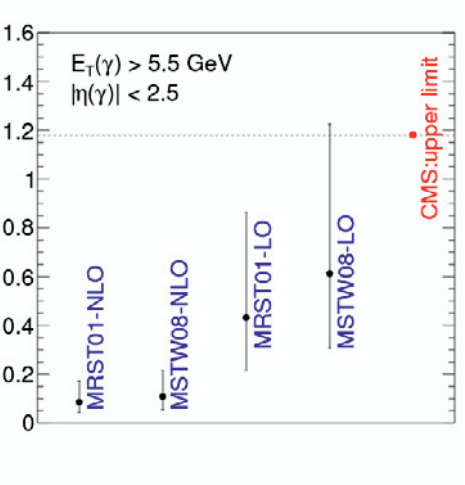

Figure 1: $pp \to p + \gamma\gamma + p$ production cross section measured by CMS and compared with ExHuMe model at LO and NLO.

CASTOR calorimeter. The data is compared to PYTHIA8-MBR simulation. The diffractive-event generation in MBR is based on a phenomenological renormalized Regge theory model, which is unitarized by interpreting a Pomeron flux as the probability for forming the diffractive rapidity gap. With an intercept for the Pomeron trajectory, $\alpha(t) = 1 + \epsilon + \alpha' t$, with $\epsilon = 0.08$ and scaling of the DD cross section downwards by 15% a good description of the data in the analysis is obtained. As a result the differential SD cross section is measured as a function of ξ, the forward momentum loss of the incoming proton, for $-5.5 < \log_{10}\xi < -2.5$ (Fig. 2). The total measured SD cross section for this region is $4.27 \pm 0.04(\text{stat.})^{+0.65}_{-0.58}(\text{syst.})$ mb.

The differential DD cross section is measured using events for which one hadronic system is detected in the central detector ($12 < M_X < 394$ GeV) and the other one in the CASTOR calorimeter ($3.2 < M_Y < 12$ GeV), as a function of $\xi_X = M_X^2/s$ for $-5.5 < \log_{10}\xi_X < -2.5$ (Fig. 2). The DD cross section is also measured differentially as a function of the width of the central pseudorapidity gap, $\Delta\eta$, for $\Delta\eta > 3$ and $M_X, M_Y > 10$ GeV. The total DD cross cross section integrated over this region is $0.93 \pm 0.01(\text{stat.})^{+0.26}_{-0.22}(\text{syst.})$ mb.

4 Hard diffraction

Diffraction with a hard scale can be described in terms of the convolution of diffractive parton distribution functions and hard scattering cross sections, calculable in pQCD. In hard-diffractive hadron-hadron collisions factorisation is broken because of soft rescattering between the spectator partons. This leads to the suppression of the observed diffractive cross section in hadron-hadron interactions. The suppression factor is called rapidity-gap survival probability. With 2010 data CMS has performed an analysis of hard diffraction events where the hard scale is set by high-p_T dijet system [4]. Events with jets with $p_T > 20$ GeV and $-4.4 < \eta < 4.4$ were selected. To enhance the diffractive contribution in the sample, the requirements on the pseudorapidity of the most forward (backward) reconstructed particle were applied: $\eta_{\max} < 3$ ($\eta_{\min} > 3$). The variables $\tilde{\xi}^+$ and $\tilde{\xi}^-$ were defined:

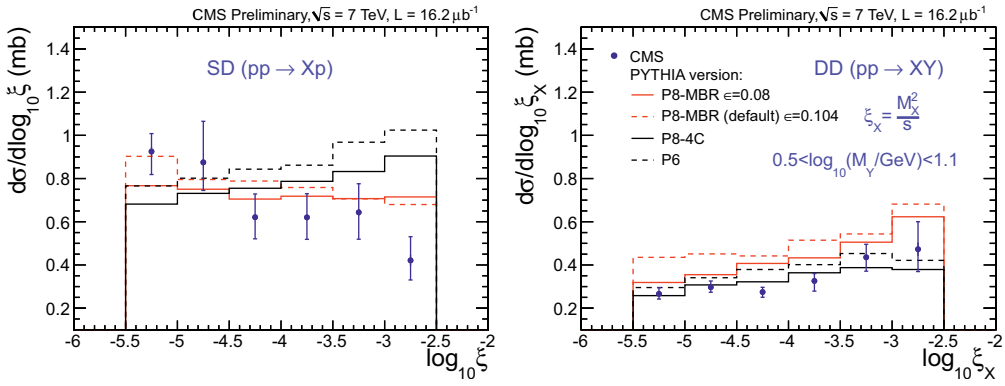

Figure 2: The SD (left) and DD (right) cross sections as a function of ξ compared to models.

$$\tilde{\xi}^{\pm} = C\frac{\sum(E^i \pm p_z^i)}{\sqrt{s}} \tag{1}$$

where E^i and p_z^i are the energy and longitudinal momentum of the i^{th} object, respectively, and the sum runs over all reconstructed objects. The C factor is a correction determined from MC and accounting for not reconstructed particles. The results are compared with the predictions of non-diffractive (PYTHIA6 Z2 and PYTHIA8 tune 1) and diffractive (POMPYT SD, POMWIG SD and PYTHIA8 SD+DD) MC generators, and with the NLO calculation based on POWHEG. The differential cross section for dijet production as a function of $\tilde{\xi}$ (averaged result for $\tilde{\xi}^+$ and $\tilde{\xi}^-$) is plotted in Fig. 3. From the comparison it is obvious that the generators without diffraction are unable to describe the data. Based on a comparison of the measured cross section with LO and NLO diffractive MCs, the rapidity-gap survival probability ranges from approximately 0.08 ± 0.04 (NLO) to approximately 0.12 ± 0.05 (LO).

5 Forward energy flow

The forward energy flow is directly sensitive to the amount of parton radiation and multiparton interaction and thus provides a measurement complementary to those for the central region alone allowing for discrimination between different models. Two measurements of the forward energy flow were performed, for HF [5] and for CASTOR [6] acceptance.

In the HF acceptance the average energy flow at forward rapidities is determined separately in two different event classes: in minimum bias events and in events with a hard scale provided by a dijet system at central rapidities ($|\eta| < 2.5$). The analysis is carried out at two different centre-of-mass energies, 900 GeV and 7 TeV. For 900 GeV (7 TeV) the leading and the sub-leading jets in the dijet system are required to have $p_T > 8$ GeV/c ($p_T > 20$ GeV/c). The measurement is restricted to $3.15 < |\eta| < 4.9$ range. The measured quantities are corrected for detector effects, and the

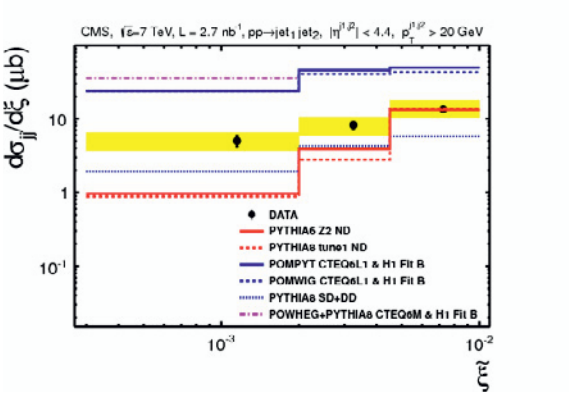

Figure 3: The differential cross section for dijet production and comparison with MC models.

distributions in the data are compared to Monte Carlo predictions on the corresponding hadron level. Both, at detector and at hadron level in MC and also in data, events are selected by requiring activity in the $3.9 < |\eta| < 4.4$ range in coincidence at both sides of CMS. This selection suppresses diffractive events. The dominant systematic effect in the measurement is the global energy scale uncertainty of the HF calorimeters, which is estimated to be 10% of the measured energy. The results are shown in Fig. 4. The systematic uncertainties are indicated as error bars, while the statistical errors are not shown since they are comparably small. The data are compared to various Monte Carlo predictions. The Pythia 6 tunes (Q^2 ordered - CW, D6T, DW, ProQ20 and p_T ordered - Z2, P0, ProPT0) are shown as bands, which are constructed from the maximum and minimum variation in the Pythia 6 predictions in each bin. The spread of forward energy flow for the different Pythia 6 tunes is fairly large, which may be a consequence of the fact that the forward region was not considered when the tunes were performed. The MC predictions without multiple interactions obtained with Pythia 6 D6T and CASCADE, undershoot the data by at least 40%. Herwig++, which uses specific tunes describes well the measurements at both energies. Pythia 8 predictions are within the tune uncertainty band of the Pythia 6.

In the CASTOR acceptance the average energy flow is measured also in the minimum bias events (defined as in the HF based analysis) and in events with a hard scale set by a dijet system in central rapidities ($|\eta| < 2$). The central jets are selected with a cut $p_T > 1$, which provides large events statistics, allowing for the energy flow measurement as a function of central jets p_T. The analysis is carried out at three different centre-of-mass energies: 900 GeV, 2.76 TeV and 7 TeV. To minimilize the systematic effects, similar for minimum bias and dijet samples, the results are presented as the ratios of energy flows in the samples at each centre-of-mass energy, Fig. 5. For 900 GeV sample the energy flow in the minimum bias sample is larger than the one measured for the dijet sample. The activity in the central region depletes the proton remnant measured in CASTOR. For 2.76 TeV the ratio is close to one, while at 7 TeV the multiple parton interactions, higher in the sample with hard scale defined, produced larger energy flow than for the minimum bias. The results are well described by Pythia 6 Z2* tune and Pythia 8 4C tune. Both were prepared including first LHC results.

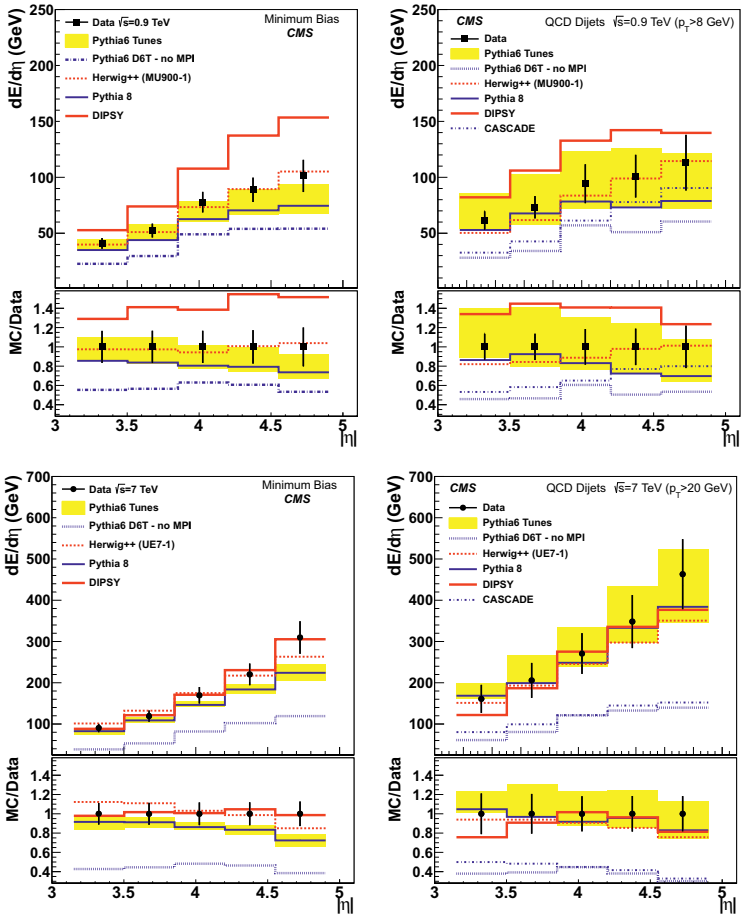

Figure 4: Forward energy flow for centre-of-mass 900 GeV (top) and 7 TeV (bottom), for minimum bias (left) and dijet (right) samples.

6 Forward and forward-central jets

The inclusive production cross sections for forward jets, as well for jets in dijet events with at least one jet emitted at central and the other at forward pseudorapidities, are measured in the range of transverse momenta p_T = 35-150 GeV/c, at centre-of-mass energy of 7 TeV [7]. Forward jets are reconstructed within $3.2 < |\eta| < 4.7$, and central jets within the $|\eta| < 2.8$ range. The jets p_T spectra are corrected to account for the migration of events across bins due to finite energy resolution of the calorimeters. Finally the corrected differential cross sections $d^2\sigma/dp_T d\eta$ are plotted. The dominant systematic uncertainty is coming from the jet energy scale in the calorimeters which propagated to the steeply falling jet spectra, translate into uncertainties of the order of $\pm(20-30)\%$ in the measured jet cross sections. The measured cross sections are compared to predictions from different pQCD approaches: (i) general-purpose event generators PYTHIA 6 with D6T and Z2 tunes, PYTHIA 8 with Tune 1, HERWIG 6 with UE modeled with JIMMY, and HERWIG++, (ii) NLO calculations

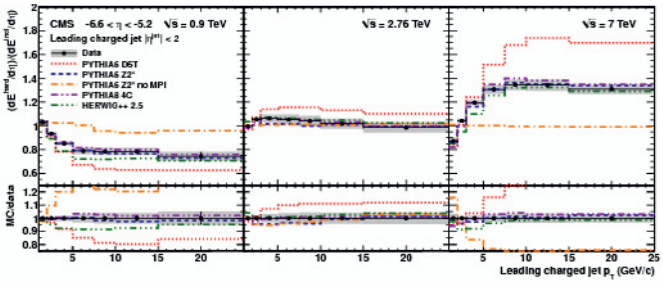

Figure 5: Ratio of the forward energy flow in CASTOR acceptance for dijet and minimum bias samples for centre-of-mass 900 GeV left , 2.76 TeV (middle) and 7 TeV (left).

obtained with the POWHEG package (matched with PYTHIA and HERWIG parton showers) as well as with NLOJET++ within the FASTNLO package, for different sets of parton densities, and (iii) the CASCADE and HEJ. Before comparing the data to parton-level predictions such as NLOJET++ or HEJ, the uncertainties from non-perturbative (NP) effects are determined, by comparing the PYTHIA 6 and HERWIG 6+JIMMY parton-level spectra with the corresponding particle-level predictions after hadronisation and UE activity. Half of the difference between the correction factors coming from these two model predictions is taken as an estimate of the total uncertainty associated with the NP effect. The uncertainty associated with higher-order corrections neglected in the NLO calculation are evaluated by changing the renormalisation and factorisation scales by factors proportional to the jet p_T ($p_T/2$ and $2p_T$). The uncertainties associated with the PDF and the strong coupling α_S is estimated following the PDF4LHC interim recommendation. The fully corrected inclusive forward jet cross section as a function of p_T is shown in Fig. 6. Within the theoretical (dark band) and systematic experimental (gray band) uncertainties, all the predictions are in agreement with the measurement. Similar plots for the cross section for the simultaneous production of at least one forward and at least one central jet are presented in Fig. 7. The HERWIG and HERWIG++ appear to be consistent with the data. The other generators, and different tunes, do not describe the data over the full range of p_T values. The discrepancies are larger for jets at central values of η. In the case of forward jets, the comparison of the inclusive p_T spectrum with that requiring the simultaneous presence of a jet in the central pseudorapidity region shows that the inclusive spectrum is about a factor of four higher in the lowest p_T bin but that both distributions agree progressively better at larger p_T values. This suggests that inclusive forward jets of $p_T \approx 35 - 70$ GeV/c may be balanced by other forward jets or by soft central jets that do not surpass the p_T threshold of 35 GeV/c, thereby producing the overall deficit of central jets in the data.

7 Ratio of inclusive to exclusive dijet production

For this studies events containing at least two jets with $p_T > 35$ GeV/c and within $|y| < 4.7$ acceptance are selected [8]. Events with at least one pair of such jets are denoted as "inclusive". Events with exactly one pair of jets are called "exclusive". The ratio of the cross section of all pairwise combinations of jets to the exclusive dijet cross section as a function of the rapidity difference between jets $|\Delta y|$ is measured (R^{inc}). The ratio of the cross section for the pair consisting of the most forward and the most backward jet from the inclusive sample to the exclusive dijet cross section is also calculated

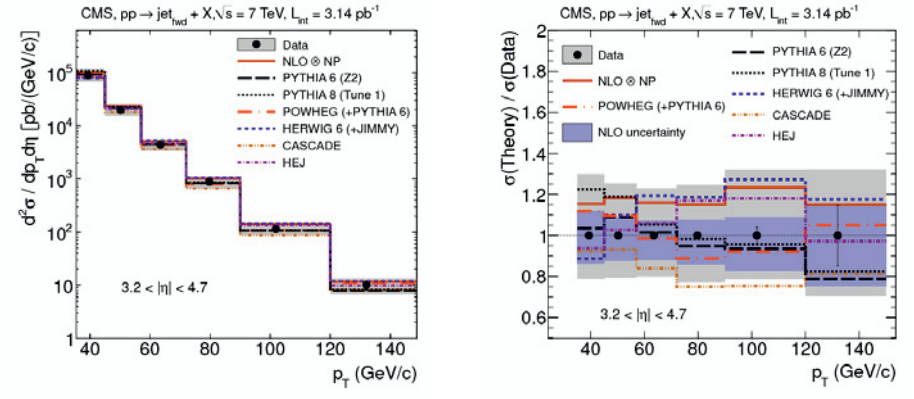

Figure 6: Inclusive jet cross section at $3.2 < \eta| < 4.7$, compared to predictions (left). Ratio of theory/data (right).

(R^{MN}). The ratios, corrected for detector effects, are compared to the MC predictions at the stable-particle level: PYTHIA6 tune Z2, PYTHIA8 tune 4C, HERWIG++ tune UE-7000-EE-3, CASCADE and HEJ+ARIADNE. The PYTHIA6 and PYTHIA8 generators agree with the measurements. The predictions of the HERWIG++ generator are larger than the measurement especially at large Δy. The BFKL-motivated generators CASCADE and HEJ+ARIADNE predict for these ratios a significantly stronger rise than observed. The moderate rise of the measured dijet ratios indicates that the BFKL effects are not dominant for jets with $p_T > 35$ GeV/c at the present collision energy of 7 TeV.

8 Mueller-Navelet dijets

A pair of the most forward and the most backward jets in an event is called Muller-Navelet dijet. Due to large rapidity separation between these jets which can be populated with soft emissions, correlation between the jets is an observable sensitive to the details of the QCD evolution. In particular BFKL effects can be disentangled from the standard DGLAP approach. The CMS analysis is based on the 7 TeV data [9]. Jets with $p_T > 35$ GeV and within $|\eta| < 4.7$ are selected. For each Muellet-Navelet pair the angular distance is calculated: $\Delta\phi = \phi_1 - \phi_2$. Then the average cosines corresponding to the coefficients of a Fourier series in $\Delta\phi$ are derived: $C_n = \langle\cos(n(\Delta - \pi))\rangle$ with $n \in \{1, 2, 3\}$. Finally the ratios between coefficients are calculated to minimilize the DGLAP and enhance BFKL effects. The results are compared to both DGLAP and BFKL-based MC generators, and to the NLL BFKL calculations. In Fig. 9 the C_2/C_1 and C_3/C_2 ratios are plotted and compared with MC models and direct NLL BFKL calculations. Standard DGLAP MC (Pythia and Herwig) describe qualitatively well the data. However the best description at large rapidity separations between jets is given by NLL BFKL calculations. This could be a first experimental indication of effects requiring the BFKL approach in the LHC regime.

References

[1] CMS Collaboration, JHEP **11**, 080 (2012)
[2] CMS Collaboration, JHEP **01**, 052 (2012)
[3] CMS Collaboration, CMS-PAS-FSQ-12-005

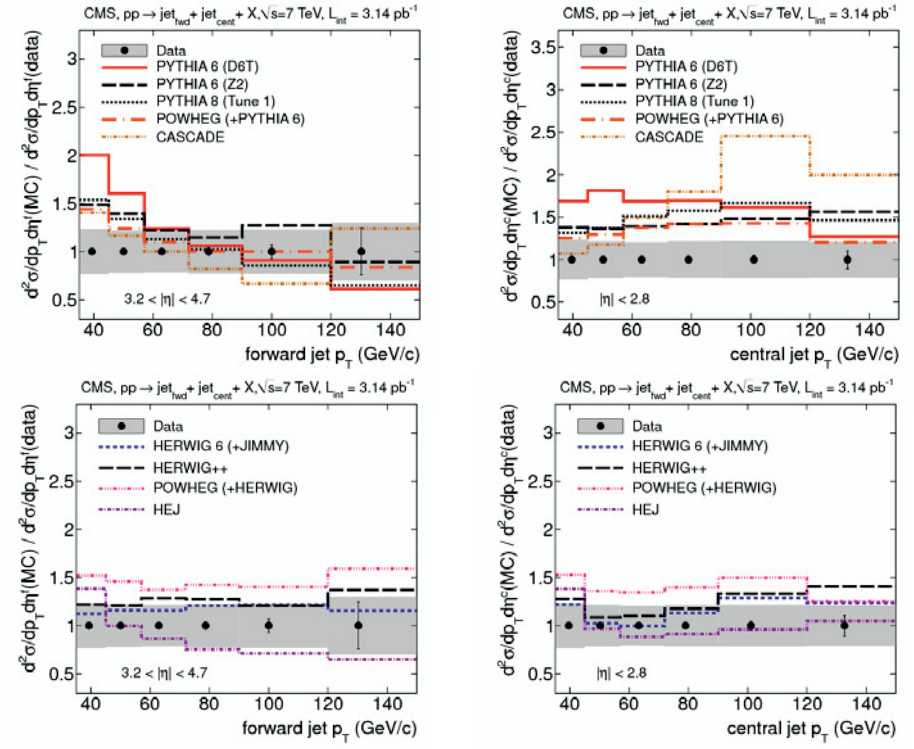

Figure 7: Theory/data for cross sections for forward (left) and central (right) jets produced in dijet events. The error bars on data points reflect statistical uncertainties, with systematic uncertainties plotted as grey bands.

[4] CMS Collaboration, Phys.Rev. D**87**, 012006 (2012)
[5] CMS Collaboration, JHEP **11** 148 (2011)
[6] CMS Collaboration, JHEP **04** 072 (2013)
[7] CMS Collaboration, JHEP **06**, 036 (2012)
[8] CMS Collaboration, Eur.Phys.J. C**72** 2216 (2012)
[9] CMS Collaboration, CMS-PAS-FSQ-12-002

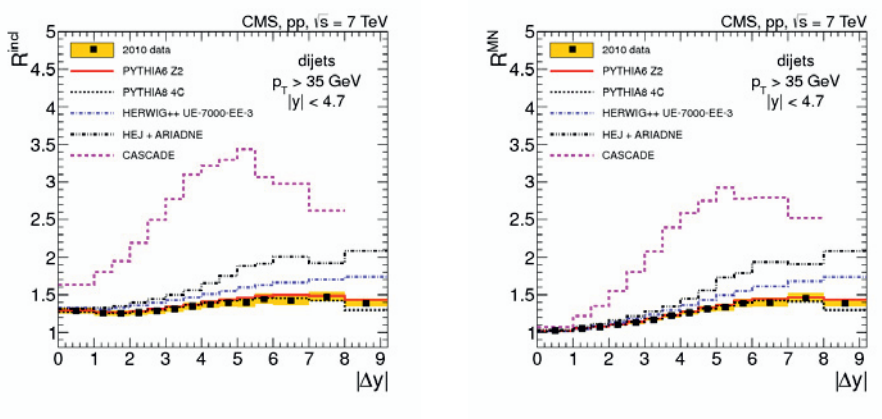

Figure 8: R^{inc} (left) and R^{MN} (right) as a function of the rapidity separation. The shaded band indicates the size of the systematic uncertainty.

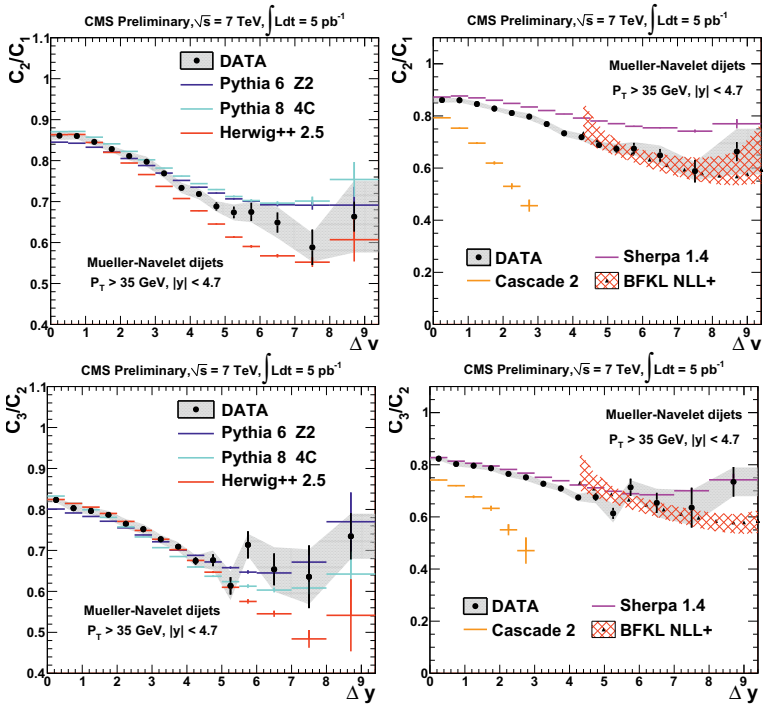

Figure 9: C_2/C_1 and C_3/C_2 ratios as a function of the separation in rapidity between jets from the Muller-Navelet pair.